HOKKAIDO UNIVERSITY

Title	Quantitative phase-field modeling for two-phase solidification process involving diffusion in the solid
Author(s)	Ohno, Munekazu; Matsuura, Kiyotaka
Citation	Acta Materialia, 58(17), 5749-5758 https://doi.org/10.1016/j.actamat.2010.06.050
Issue Date	2010-10
Doc URL	http://hdl.handle.net/2115/44154
Type	article (author version)
File Information	AM58-17_5749-5758.pdf

Instructions for use

Quantitative phase-field modeling for two-phase solidification process involving diffusion in the solid

Munekazu Ohno and Kiyotaka Matsuura

Division of Materials Science and Engineering, Faculty of Engineering, Hokkaido University, Kita 13 Nishi 8, Kita-ku, Sapporo, Hokkaido, 060-8628, Japan

Abstract

A quantitative phase-field model for two-phase solidification process is developed based on the antitrapping current approach with the free energy functional formulated to suppress the formation of an extra phase at the interface. This model appropriately recovers the free boundary problem for the motion of interface in the thin-interface limit and, importantly, it is applicable to the solidification process in binary alloy systems with arbitrary values of the solid diffusivities and interfacial energies. The performance of the present model is investigated for the peritectic reaction process in carbon steel. The present model exhibits excellent convergence behavior with respect to the interface thickness.

1. Introduction

The description of microstructures during multi-phase solidifications is one of the most important issues in materials science. The phase-field model has been emerging as a powerful model to describe a variety of microstructural evolution processes [1-3]. The diffuse interface concept in this model allows us to describe the complex morphology of the microstructure without explicitly tracking the position of the interface. Of particular relevance to the present study is the development of multi-phase-field models for multi-phase solidification processes [3-9].

The motion of solid-liquid interface has been an issue tackled in the framework of free boundary problems (FBP). Basically, the solution of the phase-field simulation must be consistent with the FBP. However, the conventional models involve several anomalous interface effects [10]. Consequently, the outcome is not consistent with the FBP and is dependent on the interface thickness, W. A seminal scheme was devised to lift this problem based on the thin-interface limit [11,12]. For the single phase solidification in binary alloy systems, the FBP can be recovered with a finite value of W by introducing an additional solute current, called the antitrapping current in the diffusion equation [12,13]. This model is called the quantitative phase-field model by which one can obtain W-independent and quantitatively accurate result under a given set of physical parameters. This quantitative phase-field model was applied to the analyses of several solidification phenomena [14-18] and it was recently

extended to the description for the multi-component alloy [19]. Importantly, a quantitative

phase-field model for two-phase solidifications was developed on the basis of the antitrapping

current scheme [20]. However, there is a limitation in the application of these models. These

models are applicable only to the alloy system without the solid diffusion (one-sided model).

Hence, one cannot reproduce the equilibrium solidification during extremely slow cooling

process and, instead, one inevitably describes the Scheil-type solidification process.

Furthermore, it is not possible to appropriately deal with the peritectic reaction and

transformation which accompanies the motion of the solid-solid interface controlled by the

solid diffusion.

Based on an asymptotic analysis, the present authors recently extended the

antitrapping current approach to the single phase solidification process involving diffusion in

the solid, viz., the case for an arbitrary value of the solid diffusivity [21]. The computations

for the dendrite growth demonstrated fairly reasonable convergence behavior of the outcomes

such as the dendrite tip velocity, dendrite tip radius and concentration profile with respect to

W. In the present study, we develop a model for two-phase solidification processes based on

this antitrapping current approach. As mentioned above, the quantitative phase-field modeling

was previously carried out for the two-phase solidification process [20]. Two notable

improvements were achieved in that modeling; one is the elimination of a problem associated

with an extra phase in the interface, which is involved in the conventional models as detailed

later, and the other is the correction of the solute concentration field by introducing the antitrapping current. The former improvement associated with the phase field profile is indispensable for the antitrapping current to work successfully in the latter improvement. As mentioned above, however, this model cannot handle the diffusion in the solid. In addition, this model is actually validated only for the system in which all two-phase interfaces possess the same interfacial energy. These are the stringent limitations in the application.

In this study, we develop the quantitative phase-field model for the two-phase solidification in binary alloy systems with arbitrary values of the solid diffusivities and interfacial energies. For this, the antitrapping current approach of Ref. [21] is extended to the case for the two-phase solidification. Also, an appropriate free energy functional is devised to remove the problem related to the extra phase at the interface. We demonstrate the performance of the present model, focusing on the peritectic reaction in carbon steel.

2. Modeling

2.1 Free energy functional

In a binary alloy system, three phases exist during the eutectic or peritectic reaction, liquid and two solid phases. We employ three phase fields, p_i, indicating the existence of i phase. The subscript i with i=1, 2 and 3 specifies the type of the phase. For generality in the discussion, also, we use indices i, j and k to distinguish the three phases. p_i is allowed to vary

from 0 to 1 and the following constraint is subjected to these phase fields,

$$\sum_i p_i = 1. \quad (1)$$

Then, for instance, the existence of i phase is represented by the relation $(p_i, p_j, p_k)=(1,0,0)$.

The j-k interface is characterized by the spatial profile of the phase fields in which p_j and p_k

smoothly vary from 1 to 0 across the interface, whereas p_i is always zero. Provided that this

spatial profile is realized, the conventional multi-phase-field model is formulated to become

identical to the model for the single phase solidification, which is the essential strategy of the

modeling. As discussed in the early studies [20, 22], however, the conventional models

involve the unexpected formation of an extra phase in the interface, More specifically, in

practice, p_i is not zero but takes a finite value inside the j-k interface region. In the description

of the motion of two-phase interface, hence, the multi-phase-field model is not consistent with

the model for the single-phase solidification. As shown later, moreover, the antitrapping

current approach does not work adequately when the unexpected extra phase exists, since the

antitrapping current term depends on the spatial profile of the phase fields. This problem

makes it impossible to perform quantitatively (and sometimes even qualitatively) accurate

simulation for the multi-phase solidifications.

In order to eliminate the extra phase, viz., in order for p_i to be zero across the j-k

interface, one must satisfy the condition, $\lim_{p_i \to 0} \partial p_i / \partial t = 0$, where t is the time. Within the

phase-field model, the time evolution of the phase field is described based on the free energy

4

functional of the system, F, as written by the following time-dependent Ginzburg-Landau equation [20],

$$\frac{\partial p_i}{\partial t} = -M\left(\{p_j\}\right)\frac{\delta F}{\delta p_i}\bigg|_{\sum p_j = 1}, \quad (2)$$

where $M(\{p_j\})$ is the mobility which depends on the phase fields. The functional derivative of F on the right-hand side of eq.(2) is evaluated with imposing the constraint of eq.(1). Using a Lagrange multiplier, the variational derivative in eq.(2) is expressed as,

$$\frac{\delta F}{\delta p_i}\bigg|_{\sum p_j = 1} = \frac{\delta F}{\delta p_i} - \frac{1}{3}\sum_j \frac{\delta F}{\delta p_j}, \quad (3)$$

where the functional derivatives on the right-hand side are taken as if all the phase fields were independent. Therefore, the condition for the elimination of the extra phase can be rewritten as,

$$\frac{\delta F}{\delta p_i}\bigg|_{\sum p_j = 1} = 0 \quad \text{at} \quad p_i = 0 \quad \forall \ i. \quad (4)$$

Specifically, the free energy functional F should be formulated to satisfy the requirement that the only steady state solution of p_i profile across the j-k interface is $p_i = 0$. Also, there is another requirement that $p_i = 1$ is the stable solution in the bulk state of any phase i. Furthermore, the stability of these solutions against a fluctuation in the phase filed profiles should be guaranteed by the condition that the second derivative of free energy is always positive at $p_i = 0$ and 1, as detailed in Ref. [20].

The condition given by eq.(4) was not taken into account in the conventional

multi-phase-field modeling. The so-called double obstacle potential with a higher order term can suppress the formation of the extra phase [22]. However, such a model is not pertinently mapped onto the thin-interface limit model. In the pioneering study on the quantitative phase-field modeling for two-phase solidifications [20], the existence of the extra phase was successfully suppressed by modifying the form of the free energy functional. However, the model presented in Ref. [22] is validated only for the system with the equal interfacial energies. Although a scheme for the description of unequal interfacial energies was proposed [20], it necessitates a revision in the available thin-interface limit analysis. No multi-phase-field model is currently developed for the system with unequal interfacial energies so as to ensure the consistency with the available quantitative phase-field model for the single phase solidification. In this section, we demonstrate the quantitative phase-field model, which is free from the problem with the extra phase in the interface and is consistent with the thin-interface limit model, for the two-phase solidification in the binary alloy system with arbitrary values of the solid diffusivities and interfacial energies. The crystalline anisotropy of the interfacial energy is not taken into account. However, the introduction of the anisotropy does not alter the essential parts in the modeling.

In this study, we propose the following form of the Ginzburg-Landau-type free energy functional,

$$F = \int \left(\frac{\varepsilon^2}{4} \sum_i (\nabla p_i)^2 + \omega(\{p_i\}) \left[\sum_i p_i^2 (1 - p_i)^2 \right] + \sum_i g_i(\{p_i\}) f_i^0(c_i, T) \right) \cdot dV . \quad (5)$$

6

where V is the unit volume. The details of each term in the integrand of eq.(5) are discussed below.

The first term in the integrand of eq.(5) represents the gradient energy term and ε is the gradient energy coefficient. It is noted that the gradient energy coefficient does not depend on the type of the two-phase interface. This is in contrast to the fact that different gradient energy coefficients are used for the different interfaces as expressed by ε_{ij} in the conventional models [4-9]. The form in eq.(5) is required to satisfy the condition given by eq. (4) [20]. The unequal interfacial energies are considered in the second term in eq.(5) as detailed below.

The second term in eq.(5), denoted here as f_{pot}, represents the potential barrier between the bulk phases, which assures that the solidification is the first order transition. The term in the square bracket represents the sum of double well potentials, $p_i^2(1-p_i)^2$. $\omega(\{p_i\})$ determines the potential height. In the conventional models [4-9], different constant values are assigned to the potential height for each interface, as expressed by ω_{ij}, to describe the unequal interfacial energies. However, the condition, eq.(4), cannot be satisfied in such an approach. If ω is taken to be a constant in eq.(5), our free energy model is essentially equivalent to the one proposed in the early work [20] for the case of the equal interfacial energies. In their work [20], in order to handle the unequal interfacial energies, the higher order term in p_i is added to the double well potential. However, such a model is not exactly reduced to the available thin-interface limit model. To deal with the unequal interface energies, in the present study,

we introduce the p_i dependence of ω. In order to hold the condition given by eq. (4), $\omega(\{p_i\})$ has to satisfy the following relation,

$$\partial\omega(\{p_i\})/\partial p_j = 0 \quad \text{at} \quad p_k = 0, 1 \quad \forall j, \quad k. \quad (6)$$

The unequal interfacial energies are introduced by holding the following relation,

$$\omega(\{p_i\}) = \tfrac{1}{2}\omega_{ij} \quad \text{at} \quad p_k = 0, \quad (7)$$

where ω_{ij} denotes the potential height between i and j phases. In this study, we define $\omega(\{p_i\})$ as follows,

$$\omega(\{p_i\}) = \left(2\sum_{i,j>i} p_i^2 p_j^2\right)^{-1}\left(\sum_{i,j>i}\omega_{ij}\cdot p_i^2 p_j^2 + \omega_{tri}\cdot\left(p_i p_j p_k\right)^n\right), \quad (8)$$

with $n>1$. Here, ω_{tri} is a constant related to the potential height for the mixture state of three phases. It is trivial to check that $\omega(\{p_i\})$ in eq.(8) satisfies eqs.(6) and (7). Note that f_{pot} is exactly reduced to the corresponding term in the available thin-interface limit model for the single phase solidification [21] at $p_k=0$. The function $\omega(\{p_i\})$ exhibits a discontinuity at $p_k=1$ as $\lim\limits_{p_k\to 1}\omega(\{p_i\}) = (1/2)(\omega_{jk}p_j^2+\omega_{ki}p_i^2)/(p_j^2+p_i^2)$. However, the discontinuity vanishes in f_{pot} and there is no problem in the numerical simulations. In eq.(8), the term multiplied by ω_{tri} plays an auxiliary role in raising the potential height for the mixture state of three phases, of which the contribution is determined by ω_{tri} and n. Our preliminary calculations showed that this term is quite useful in suppressing the formation of the extra phase when the difference between the interfacial energies is large. It should be stressed that the unequal interfacial energies are considered in f_{pot} which satisfies the condition of eq.(4) and keeps the consistency

with the available quantitative phase-field model.

The third term in the integrand of eq.(5) represents the contribution of the free energies of the bulk phases, yielding the driving force for the solidification. $f_i^0(c_i,T)$ is the free energy density of i phase given as a function of the concentration of i phase, c_i, and temperature T. $g_i(\{p_i\})$ is the interpolating function and we adopt the following form devised in the early work [20],

$$g_i(\{p_i\}) = \frac{p_i^2}{4}\left\{15(1-p_i)\left[1+p_i-(p_k-p_j)^2\right]+p_i(9p_i^2-5)\right\}, \quad (9)$$

This function $g_i(\{p_i\})$ reduces to the polynomial $\widetilde{g}(p_i)=p_i^3(10-15p_i+6p_i^2)$ on i-j and i-k interfaces when the normalization condition eq.(1) is imposed [20].

As mentioned above, the free energy functional proposed in this study is formulated to remove the extra phase in the interface and this model can deal with the unequal interfacial energies. It should be noticed that when $p_k=0$, this free energy functional reads

$$F = \int\left(\frac{\varepsilon^2}{2}(\nabla p_i)^2 + \omega_{ij}p_i^2(1-p_i)^2 + \widetilde{g}(p_i)f_i^0(c_i,T)+(1-\widetilde{g}(p_i))f_j^0(c_j,T)\right)\cdot dV. \quad (10)$$

This is exactly the same as the free energy functional proposed in the quantitative phase-field modeling for the single phase solidification [21].

2.2. Time evolution equations

As mentioned in the previous section, the time evolution of phase fields is described by the time-dependent Ginzburg-Landau equation (2). In the free energy functional given in

eq.(5), three concentration fields, $\{c_i\}$, are used as the variables. As in the conventional

multi-phase-field models [6-9], these concentrations obey the mixture rule, $c=\Sigma p_i c_i$. Also,

following Kim, Kim, Suzuki's (KKS) model [23], the condition for the equal chemical

potential, $\partial f_i/\partial c_i = \partial f_j/\partial c_j = \partial f_k/\partial c_k = \mu_c$, is introduced to make the steady state profiles of the

phase fields independent of the concentration fields in the interface region. Then, the

functional derivative of F on the right-hand side of eq.(3) is written as,

$$\frac{\delta F}{\delta p_i} = -\frac{1}{2}\varepsilon^2\nabla^2 p_i + 2\omega(\{p_i\})p_i(1-p_i)(1-2p_i)$$

$$+\frac{\partial\omega(\{p_i\})}{\partial p_i}\left(\sum_j p_j{}^2(1-p_j)^2\right)+\sum_j \frac{\partial g_j}{\partial p_i}\left(f_j - \mu_c c_j\right). \quad (11)$$

The last term on the right-hand side of eq.(11) represents the thermodynamic driving force for

the solidification. In dilute solution limit, the driving force term can be approximated as,

$$f_j - \mu_c c_j \approx v_m{}^{-1}RT\left(-c_{k,e}^j + c_{j,e}^k - c_j\right), \quad (12)$$

where v_m is the molar volume, R is the gas constant and $c_{j,e}^k$ is the concentration in j phase in

equilibrium with k phase. In the expression of eq.(12), k phase corresponds to a reference

phase. When $j=k$, $f_k-\mu_c c_k$ is given as $-v_m{}^{-1}RTc_k$. In our numerical computation, the reference

phase was chosen to be the liquid phase.

The time evolution equation (2) is different from the one in the conventional model

in the light of the fact that a different value is assigned to the mobility for different two-phase

interface in the conventional model. In eq.(2), we introduced the dependence of the mobility

on the phase field in order to handle the different mobility for the different interface without

10

the formation of the extra phase [20]. $M(\{p_j\})$ is defined in this study as follows,

$$M(\{p_j\}) = 2\left(\sum_{i,j>i} M_{ij} p_i p_j\right)\left(\sum_{i,j>i} p_i p_j\right)^{-1}, \quad (13)$$

where M_{ij} is the mobility for i-j interface. When $p_k = 0$, $M(\{p_i\})$ is given as $M(\{p_i\}) = 2M_{ij}$. This

function contains the discontinuity at $p_k = 1$. However, it does not cause any problem in

practice.

The time evolution of the concentration field, c, is described by the following

diffusion equation,

$$\frac{\partial c}{\partial t} = -\nabla(\mathbf{J}_c + \mathbf{J}_{at}), \quad (14)$$

where $\mathbf{J}_c$ is the solute flux and $\mathbf{J}_{at}$ is the antitrapping current. $\mathbf{J}_c$ is given as [6],

$$\mathbf{J}_c = -D(\{p_i\})\sum_i p_i \nabla c_i, \quad (15)$$

where $D(\{p_i\})$ is the diffusion coefficient of p_i dependent. In this study, we use the relation

$c_i = k_{ij} c_j$ with the partition coefficient $k_{ij} = c_i/c_j$, since our focus is placed on the dilute solid

solution. To keep the consistency with the single phase solidification model [21], in this study,

we define $D(\{p_i\})$ as follows,

$$D(\{p_i\}) = \left(\sum_i D_i k_{ij} p_i\right)\left(\sum_i k_{ij} p_i\right)^{-1}, \quad (16)$$

with a reference phase j. D_i is the diffusion coefficient of solute element in i phase. Then, the

solute flux is expressed by the relatively simple form,

$$\mathbf{J}_c = -\sum_i D_i p_i \nabla c_i. \quad (17)$$

An assumption should be necessarily introduced in the extension of the antitrapping current approach to the two-phase solidification process, since no thin-interface limit analysis is available for the mixture state of three phases. We tested several possibilities for this extension and found that the approach proposed in Ref. [20] results in the best convergence behavior. Then, in this study, the antitrapping current for an arbitrary value of the solid diffusivity [21] is extended as follows,

$$\mathbf{J}_{at} = -2\sum_{i,j>i}\left(\mathbf{n}_i \cdot \mathbf{n}_j\right)a_{ij}\frac{\varepsilon}{\sqrt{\omega_{ij}}}\left(c_j - c_i\right)\frac{\partial p_i}{\partial t}\mathbf{n}_i, \quad (18)$$

where $\mathbf{n}_i$ denotes the unit vector normal to the contour surface of p_i phase field as given by $\mathbf{n}_i = -\nabla p_i/|\nabla p_i|$. a_{ij} is the coefficient of which the form depends on the type of interpolating functions used in the model. In the present model, the coefficient a_{ij} is given by [21],

$$a_{ij} = \frac{1}{2\sqrt{2}}\left[D_j - k_{ij}D_i\right]\Psi_{ij}\left(\chi_{ij}\right), \quad (19)$$

with

$$\Psi_{ij}\left(\chi_{ij}\right) = 1 - \frac{1}{2}\left[1 - k_{ij}D_i/D_j\right]\chi_{ij}, \quad (20)$$

where χ_{ij} is a quantity associated with the solute concentration field at the *i-j* interface. As discussed in Ref. [21], in this approach, χ_{ij} is regarded as a parameter controlling the convergence behavior of the output with respect to the interface thickness, *W*.

The most important fact in the present model is that the equations (2) and (14) reduce to the following equations at $p_k=0$,

$$\frac{1}{M_{ij}}\frac{\partial p_i}{\partial t} = \varepsilon^2 \nabla^2 p_i - 2\omega_{ij} p_i (1 - p_i)(1 - 2p_i) - 30 p_i^2 (1 - p_i)^2 \left(f_i - f_j - (c_i - c_j)\mu_c \right), \quad (21)$$

$$\frac{\partial c}{\partial t} = \nabla \left[\left(D_j + (D_i k_{ij} - D_j) p_i \right) \nabla c_j + 2a_{ij} \frac{\varepsilon}{\sqrt{\omega_{ij}}} (c_j - c_i) \frac{\partial p_i}{\partial t} \frac{\nabla p_i}{|\nabla p_i|} \right]. \quad (22)$$

These equations are exactly identical to those in the quantitative phase-field model developed in Ref. [21]. It should not be necessary to repeat here the asymptotic analysis of these equations. It was demonstrated in Ref. [21] that the model given by eqs. (21) and (22) can be mapped onto the FBP in the thin-interface limit and it allows the quantitatively accurate simulation with a finite value of *W*. Compared with the earlier work in Ref. [20], the present model is advantageous in terms of the fact that the solid diffusions and the unequal interfacial energies are taken into account.

2.3. Relationships between parameters

The relationships between the phenomenological parameters in the phase-field model and the measurable quantities are discussed. For a planar *i-j* interface, the steady state profile of p_i phase field is analytically expressed by solving eq.(21) as follows,

$$p_i = \frac{1}{2}\left(1 - \tanh\left(\frac{x}{\sqrt{2}W_{ij}} \right) \right), \quad (23)$$

where $W_{ij} = \varepsilon/(\omega_{ij})^{1/2}$ corresponds to the thickness of *i-j* interface. Also, the *i-j* interfacial energy, σ_{ij}, is represented by

$$\sigma_{ij} = \frac{1}{3\sqrt{2}} \varepsilon \sqrt{\omega_{ij}} . \quad (24)$$

13

It is noted that ε does not depend on the type of interface and, hence, W_{ij} should be chosen so that the product $\sigma_{ij}W_{ij}$ is independent of the type of interface. Then, ε and ω_{ij} are uniquely determined under a given set of σ_{ij}.

According to the thin-interface limit analysis, the mobility M_{ij} is given, under the condition of vanishing kinetic coefficient, as follows [21],

$$M_{ij} = \left(\frac{15}{4} \frac{a_2 \cdot \varepsilon^2}{\omega_{ij} \cdot D_j} \frac{RT_{m,ij}}{v_m} \left(1 - k_{ij}\right)\left(c_{j,e}^i - c_{i,e}^j\right)\Psi_{ij}\left(\chi_{ij}\right) \right)^{-1}, \quad (25)$$

where $T_{m,ij}$ is the transition temperature between i and j phases of pure element and a_2 is the constant depending on the forms of interpolating functions used in this model and it is given in the present model as $a_2 = 0.6276\cdots$.

3. Computational details

We carried out the simulation for the peritectic reaction of carbon steel, liquid(L)+ferrite(δ)→austenite(γ), based on the present model to check the convergence behavior of the output with respect to the interface thickness, W_{ij}. For convenience, in the following discussion, we use the notation γ, δ and L for the index in variable such as $p_{L,}$ $\sigma_{\gamma\delta}$ instead of $i=1$, 2 and 3.

Equations (2) and (14) were discretized based on standard second-order finite difference formula with the squire grid spacing, Δx. We performed two-dimensional simulations for the isothermal peritectic reaction process, focusing on the growth of plate-like

γ phase. The system of our focus is schematically illustrated in Fig. 1. The system has a

square shape with zero flux boundary condition along all the boundaries. The edge lengths are

denoted by W_x and W_y. There is a flat δ-L interface. The initial concentrations of δ and L

phases are given as $c_{\delta,e}^L$ and $c_{L,e}^\delta$, respectively, at the holding temperature. In the initial state,

there is a semicircular γ phase with a diameter, d_i, and a concentration, c_γ^0.

The γ phase grows along the δ-L interface (y direction). The velocity of the front

edge of the growing γ phase, viz., the peritectic reaction rate was calculated at several degrees

of undercooling from the peritectic reaction temperature, ΔT, until the steady state was

realized. Our preliminary simulations showed that the velocity takes almost a constant value

typically after $t=2.0\times10^{-4}$s for $\Delta T=5$ K and $t=1.0\times10^{-4}$s for $\Delta T=10$ K. The time step was set to

be $\Delta t=5\times10^{-11}$–2×10^{-10}s, depending on Δx and ΔT. It was observed in our preliminary

simulations that small system size incurs a size effect that the steady state velocity

appreciably depends on the values of W_x and W_y. The values of W_x and W_y were accordingly

chosen in each condition to be large enough to avoid such a size effect. On the other hand, the

values of c_γ^0 and d_i were found to be irrelevant to the steady state velocity. In all the

calculations presented here, we employed $c_\gamma^0=c_{\gamma,e}^L$ and $d_i=40\times10^{-8}$ m. The interface

thicknesses were set to be $W_{\gamma\delta}=2.0\times\Delta x$, $W_{\delta L}=\sigma_{\gamma\delta}W_{\gamma\delta}/\sigma_{\delta L}$ and $W_{\gamma L}=\sigma_{\gamma\delta}W_{\gamma\delta}/\sigma_{\gamma L}$. ω_{tri} in eq.(8)

was given as $\omega_{tri}=\omega_{\delta L}+\omega_{\gamma L}+\omega_{\gamma\delta}$, unless otherwise stated. The parameter χ_{ij} was set to be $\chi_{ij}=0$

for all the interfaces. The computation with $\chi_{ij}=0$ yields quite reasonable convergence

behavior for the dendrite growth [21] and this is also the case for the peritectic reaction, as demonstrated in the next section. The other input parameters employed in this study are listed in Table 1.

4. Results and discussion

As described in the introduction, the conventional models involve the anomalous interface effects and the magnitude of these effects scales with the interface thickness. Shown in Fig. 2 is the dependence of the growing velocity of γ phase (peritectic reaction rate), V_p, on the interface thickness $W_{\gamma\delta}$. The degree of undercooling is ΔT=10 K. In these calculations, the thicknesses of the δ-L and γ-L interfaces were also varied according to the relations $W_{\delta L}=\sigma_{\gamma\delta}W_{\gamma\delta}/\sigma_{\delta L}$ and $W_{\gamma L}=\sigma_{\gamma\delta}W_{\gamma\delta}/\sigma_{\gamma L}$ as discussed in the previous section. The values of ε, ω_{ij}, ω_{tri} and M_{ij} were varied accordingly. The system size was chosen to be $W_x \geq 4\times10^{-6}$ m and $W_y \geq 2\times10^{-6}$ m. Three types of square symbols represent the results calculated with the assumption of the equal interfacial energies, $\sigma_{\delta L}= \sigma_{\gamma L}= \sigma_{\gamma\delta}$=2.04 J·m^{-2}. The full square and half-open square symbols indicate the results for n=1.4 and n=2.0, respectively. The reason for the choice of the special value, n=1.4, will be explained later. The open square symbols represent the results for n=0.0 and ω_{tri}=0.0. In this case, the model is actually equivalent to the model of Ref. [20], except that the solid diffusions are taken into account in the present model. One can see that all the results merge into almost the single curve as the interface thickness decreases.

However, a well converged value seems to be not achieved even for the smallest value of $W_{\gamma\delta}$ tested here. Importantly the convergence behavior depends on the value of n. The simulation with $n=1.4$ yields the most reasonable convergence behavior. It is noticed that the extra phase does not form in each interface region in the simulation for the equal interfacial energies. The difference in the convergence behavior originates from the difference in the potential height for the mixture state of three phases which is called the additional potential here. Among these cases, the additional potential height is the lowest in the simulation for $n=0.0$ and is the highest for $n=1.4$. Hence, it is seen that the increase in the additional potential height leads to the better convergence behavior, which should be ascribable to narrowing of the region for the mixture state of three phases near the triple junction.

Three types of the circular symbols in Fig. 2 indicate the velocities calculated with the unequal interfacial energies listed in Table 1. The results for $n=1.4$ and $n=2.0$ are shown by full and half-full circle symbols, respectively. Also, the results for $n=0.0$ and $\omega_{tri}=0.0$ are indicated by the open symbols. The simulation with the unequal interfacial energies involves the problem associated with the extra phase in the interface. Especially, the extra phase is prone to form in the interface of the highest interfacial energy, specifically, the $\gamma-\delta$ interface in this system. The phase field profiles across the $\gamma-\delta$ interface far from the triple junction are shown in Fig. 3(a). The result for $n=1.4$ and $W_{\gamma\delta}=1.0\times10^{-8}$ m is presented in Fig. 3(a). The enlargement of the phase field profiles in the vicinity of $p_i=0$ is shown in Fig. 3(b) where the

profiles of p_L for n=0.0 and 2.0 are added. It is seen that the spatial profile of p_L depends on

the value of n. When there is no additional potential (n=0.0 and ω_{tri}=0.0), the extra phase

exists in the γ–δ interface. The peak position of p_L is located not at the center of the γ–δ

interface but on the δ phase side. In other words, the δ-L interface configuration appears

inside the γ-δ interface. This is because the δ-L interface possesses the lowest interfacial

energy in this system and it incurs the tendency of the δ-L interface configuration to form.

The maximum value of p_L is reduced by introducing the additional potential (n=2.0). Most

importantly, the extra phase vanishes for n=1.4. It is clear in Fig. 2 that the simulation for

n=1.4 exhibits the excellent convergence behavior.

In Fig. 3(b), the peak value of p_L for n=0.0 is higher than the one for n=2.0. However

the difference in the peak value is not significantly large. Therefore, there is actually only a

slight difference between these cases in the migration velocity of the γ–δ interface far from

the triple junction. The appreciable difference between the peritectic reaction rates in Fig. 2

(especially at $W_{\gamma\delta}$=1.0×10^{-8}m) originates from the formation of the extra phase near the triple

junction. For this discussion, we employ the square sum of phase fields, p_s=p_L^2+p_δ^2+p_γ^2. p_s

varies from 0.5 to 1.0 across the two-phase interface and it takes the minimum value of p_s=1/3

at the triple junction. The contour lines of p_s near the triple junction for n=0.0, 1.4 and 2.0 are

shown in Fig. 4. These are the results calculated with $W_{\gamma\delta}$=1.0×10^{-8}m. The solid lines indicate

the level 0.5 contour lines of phase fields. The cross-hatched region represents the region for

$p_s \le 0.5$ and, hence, the mixture state of three phases forms in this region. It is clear that the

mixture state is confined into a narrow region when the additional potential contribution is

large (Fig. 4(b)). When the contribution of the additional potential is reduced (Fig. 4(c)), the

region for the mixture state is extended to each interface region and especially to the $\gamma-\delta$

interface region. When the addition potential is removed (Fig. 4(a)), the region for the mixture

state is substantially extended to the γ-δ interface region. Then, the motion of the interface in

this region cannot be appropriately described due to the existence of the extra phase. The

antitrapping current does not properly work and the anomalous interface effects become

significant in this region. As a result, the peritectic reaction rate calculated for $n=0.0$ is quite

different from those for $n=2.0$ and 1.4 even for the smallest value of $W_{\gamma\delta}$ in Fig. 2. In addition,

as detailed in the supplementary material, the formation of the extra phase cannot be

suppressed only by decreasing the interface thickness when the additional potential is not

introduced. In Fig. 2, therefore, the result for $n=0.0$ seems to be converged to a different value

from the one for $n=1.4$.

In the present model, the contribution of the additional potential increases with the

decrease in n and with the increase in ω_{tri}. As discussed in the supplementary material, the

formation of the extra phase can be effectively suppressed by using the small value of n

and/or the larger value of ω_{tri} in the present model. The convergence behavior can be thereby

improved. However, when the contribution of the additional potential is too large, the

calculation becomes unstable. When we tried $n=1.2$ and 1.3 with $\omega_{tri}=\omega_{\delta L}+\omega_{\gamma L}+\omega_{\gamma\delta}$, the calculations were not stable. Since the excellent convergence was demonstrated for $n=1.4$ and $\omega_{tri}=\omega_{L\delta}+\omega_{L\gamma}+\omega_{\delta\gamma}$, we employed these values in the following calculations.

The dependence of V_p at $\Delta T=10$ K on $W_{\gamma\delta}$ is shown in Fig. 5(a). These are the results for the unequal interfacial energies. For comparison, we performed the same simulation based on a model without the antitrapping current and with $D(\{p_i\})=D_L p_L+D_\delta p_\delta+D_\gamma p_\gamma$ in eq.(15), which is called the standard model here. It is noted that this standard model is free from the problem of the extra phase in the interface, while it involves the spurious interface effects in the motion of the two-phase interface (chemical potential jump at the interface and surface diffusion). It is seen that the present model exhibits the well-converged value even for a relatively large value of $W_{\gamma\delta} =3.0\times10^{-8}$ m. On the other hand, the result of the standard model largely depends on the interface thickness and the result is not well converged even for the smallest value of $W_{\gamma\delta} =1.0\times10^{-8}$ m tested here. The same simulations were performed for $\Delta T=5$ K and the results are shown in Fig. 5(b). The system size was chosen to be $W_x\geq6\times10^{-6}$m and $W_y\geq3\times10^{-6}$m. The smallest value of $W_{\gamma\delta}$ was set to be 2.0×10^{-8} m in the light of the computational burden. It is again demonstrated that the convergence behavior obtained by the present model is excellent as compared with that by the standard model.

The steady state shape of the interfaces near the triple junction at $\Delta T=10$ K is shown in Fig. 6 (a). The origin of y axis corresponds to the center of triple junction and the origin of

x axis is the initial position of δ-L interface. These lines represent the level 0.5 contour lines of phase fields. The shape of the interfaces near the triple junction is almost independent of the interface thickness in the present model, while the results of the standard model depend on the interface thickness. In Fig. 6(a), the deviation of the δ−L interface from the initial position indicates the melting of δ phase near the growth front of γ phase. This steady state shape near the junction represents the well-known feature in the peritectic reaction process, as recently demonstrated in the quantitative phase-field simulation without the solid diffusion [29]. More detailed analysis on the peritectic reaction in the carbon steel is reported elsewhere [30].

Figure 6 (b) shows the concentration profiles along *x* direction at *y*=−0.3 μm. The circular and square symbols represent the results of the present and the standard models, respectively. One can see that the concentration profiles are also independent of the interface thickness in the present model.

As demonstrated above, the present model exhibits the excellent convergence behavior of the outcomes with respect to the interface thickness. Although the detail is not discussed here, it was confirmed that the present model successfully reproduces the equilibrium relation of contact angles between interfaces near the triple junction described by Young's rule within an accuracy of less than 1° near the peritectic temperature [30].

5. Conclusions

In this study, we developed the quantitative phase-field model for two-phase solidification processes. This model is consistent with the available quantitative phase-field model for the single phase solidification. Hence, the free boundary problem is recovered with a finite value of interface thickness in describing the motion of the interfaces. Importantly, this model can be applied to the system with arbitrary values of the solid diffusivities and interfacial energies. In this study, we investigated the performance of this model, focusing on the peritectic reaction in the carbon steel. The excellent convergence behavior of the outcome was demonstrated. The extension of the present approach to the multi-component system is quite important task for a step further to the development of effective computational tool to quantitatively describe the microstructural evolution processes.

Acknowledgments

References

[1] A. Karma, Encyclopedia of Materials Science and Technology (Elsevier, Oxford, 2001).

[2] L.-Q. Chen, Annu Rev Mater Sci 2002;32;113.

[3] I. Steinbach, Modelling Simul Mater Sci Eng 2009;17; 073001.

[4] I. Steinbach, F. Pezzola, B. Nestler, M. Seeßelberg, R. Prieler, G.J. Schmitz and J.L.L. Rezende, Physica D 1996;94;135.

[5] I. Steinbach and F. Pezzola, Physica D 1999;134;385.

[6] S.G. Kim, W.T. Kim, T. Suzuki, M. Ode, J Cryst Growth 2004;261;135.

[7] B. Boettger, J. Eiken and I. Steinbach, Acta Mater 2006;54;2697.

[8] R.S. Qin, E.R. Wallach and R.C. Thomson, J Cryst Growth 2005;279;163.

[9] J. Eiken, B. Böttger and I. Steinbach, Phys Rev E 2006;73;0666122.

[10] R.F. Almgren, SIAM J Appl Math 1999;59;2086.

[11] A. Karma and W.-J. Rappel, Phys Rev E 1998;57;4323.

[12] A. Karma, Phys Rev Lett 2001;87;115701.

[13] B. Echebarria, R. Floch, A. Karma and M. Plapp, Phys Rev E 2004;70;061604.

[14] J.C. Ramirez, C. Beckermann, A. Karma and H.-J. Diepers, Phys Rev E 2004;69;051607.

[15] M. Greenwood, M. Haataja and N. Provatas, Phys Rev Lett 2004;69;051607.

[16] C.W. Lan and C.J. Shih, Phys Rev E 2004;69;031601.

[17] J.C. Ramirez and C. Beckermann, Acta Mater 2005;53;1721.

[18] A. Badillo and C. Beckermann, Acta Mater 2006; 54; 2015.

[19] S.G. Kim, Acta Mater 2007;55;4391.

[20] R. Folch and M. Plapp, Phys Rev E 2005; 72;011602.

[21] M. Ohno and K. Matsuura, Phys Rev E 2009;79;031603.

[22] H. Gracke, B. Nestler and B. Stoth, SIAM J Appl Math, 1999;60;295.

[23] S.G. Kim, W.T. Kim and T. Suzuki, Phys Rev E 1999;60;7186.

[24] W. Kurz and D.J. Fisher, Fundamentals of Solidification, Trans Tech Publication (Switzerland, 1989).

[25] Y. Sun, M. Asta, J.J. Hoyt, M.I. Mendelev and D.J. Srolovitz, Phys Rev B 2004;69;020102(R).

[26] H. Yin, T. Emi and H. Shibata, Acta Mater 1999;47;1523.

[27] T. Matsumiya, H. Kajioka, S. Mizoguchi, Y. Ueshima and H. Esaka, Trans ISIJ 1984;24;873.

[28] P. Gustafson, Scand J Metall 1985;14;259.

[29] G. Boussinot, E.A. Brener, D.E. Temkin, Acta Mater 2010;58;1750.

[30] M. Ohno and K. Matsuura, (submitted).

Table 1 Input parameters for Fe-C system used in the present study

Quantity	Symbol	Value used
Molar volume	v_m	7.7×10^{-6} m^3/mol [24]
Partition coefficient of δ–L phases	$k_{\delta L}$	0.179[*)]
Partition coefficient of γ–L phases	$k_{\gamma L}$	0.334[*)]
Partition coefficient of γ–δ phases	$k_{\gamma \delta}$	$k_{\gamma L}/k_{\delta L}$
Melting temperature of pure bcc-Fe	$T_{m,\delta L}$	1811 K[*)]
Melting temperature of pure fcc-Fe	$T_{m,\gamma L}$	1801 K[*)]
δ/γ transition temperature of pure Fe	$T_{m,\gamma \delta}$	1399 K[*)]
Liquidus slope of δ phase	m_δ	1828 K/mol fraction[*)]
Liquidus slope of γ phase	m_γ	1399 K/mol fraction[*)]
Interfacial energy of δ-L boundary	$\sigma_{\delta L}$	0.204 J/m^2[24]
Interfacial energy of γ-L boundary	$\sigma_{\gamma L}$	0.319 J/m^2 [25]
Interfacial energy of γ-δ boundary	$\sigma_{\delta \gamma}$	0.370 J/m^2 [26]
Diffusion coefficient in L phase	D_L	$5.2 \times 10^{-7} \cdot \exp(-5.0 \times 10^4 \cdot \beta)$ m^2/s[**)] [27]
Diffusion coefficient in δ phase	D_δ	$1.27 \times 10^{-6} \cdot \exp(-8.3 \times 10^4 \cdot \beta)$ m^2/s[**)] [27]
Diffusion coefficient in γ phase	D_γ	$7.61 \times 10^{-6} \cdot \exp(-13.7 \times 10^4 \cdot \beta)$ m^2/s[**)] [27]

[*)]These values were estimated from the thermodynamic assessment of Ref. [28]. [**)] $\beta = (R \cdot T)^{-1}$
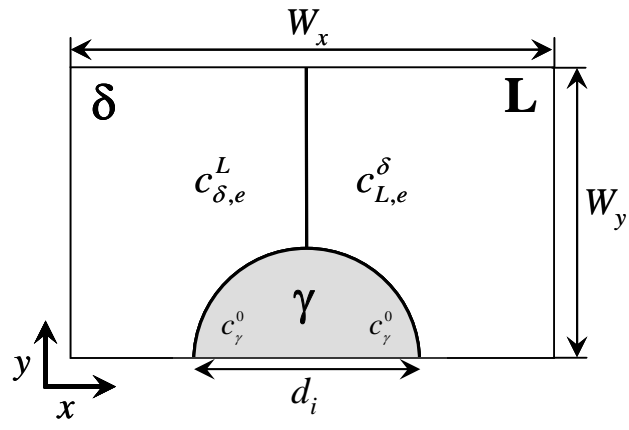
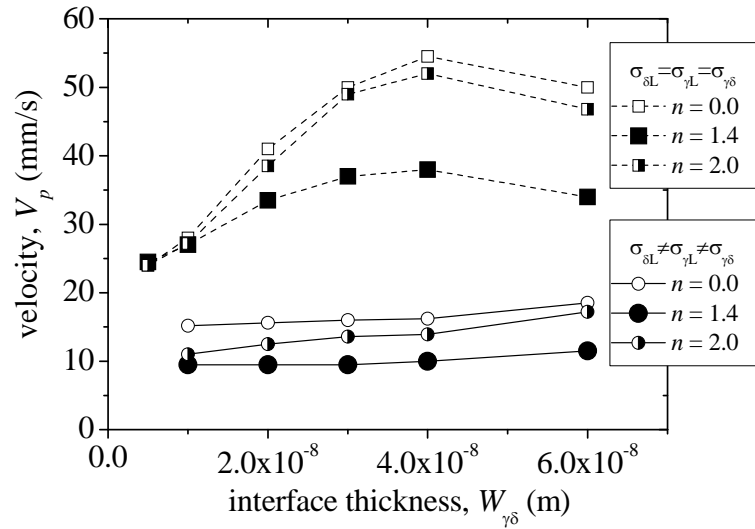Fig. 1. Schematic illustration of the initial state in two-dimensional system used in this study.

Fig. 2. Dependence of the growing velocity of γ phase on interface thickness, $W_{\gamma\delta}$, calculated for n=0.0 (open symbols), n=1.4(full symbols) and n=2.0 (half-full symbols). The degree of undercooling is ΔT=10 K. The square symbols correspond to the results for equal interfacial energies, while the circular symbols represent those for unequal interfacial energies.
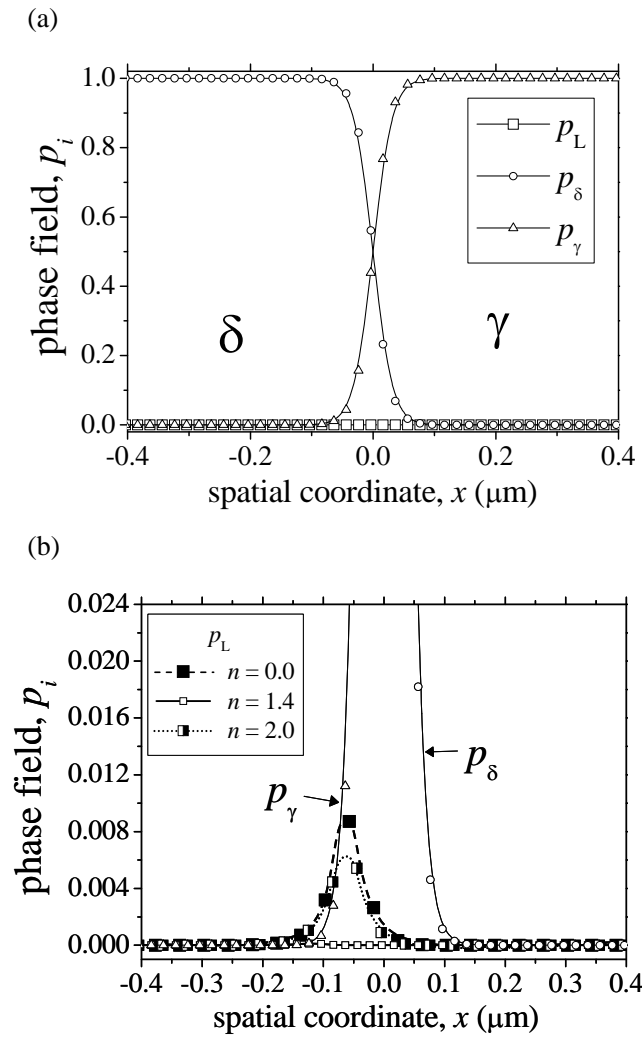
(a)

(b)

Fig. 3 (a) Phase field profiles across γ–δ interface along x direction calculated for n=1.4 and $W_{\gamma\delta}$=1.0×10^{-8} m at ΔT=10 K. For visual aid, one out of every 4 symbols is shown for each profile. (b) Enlargement of profile in the vicinity of p_i=0 where p_L profiles for n=0.0 and n=2.0 are also shown. One of every 8 symbols is shown for these profiles.
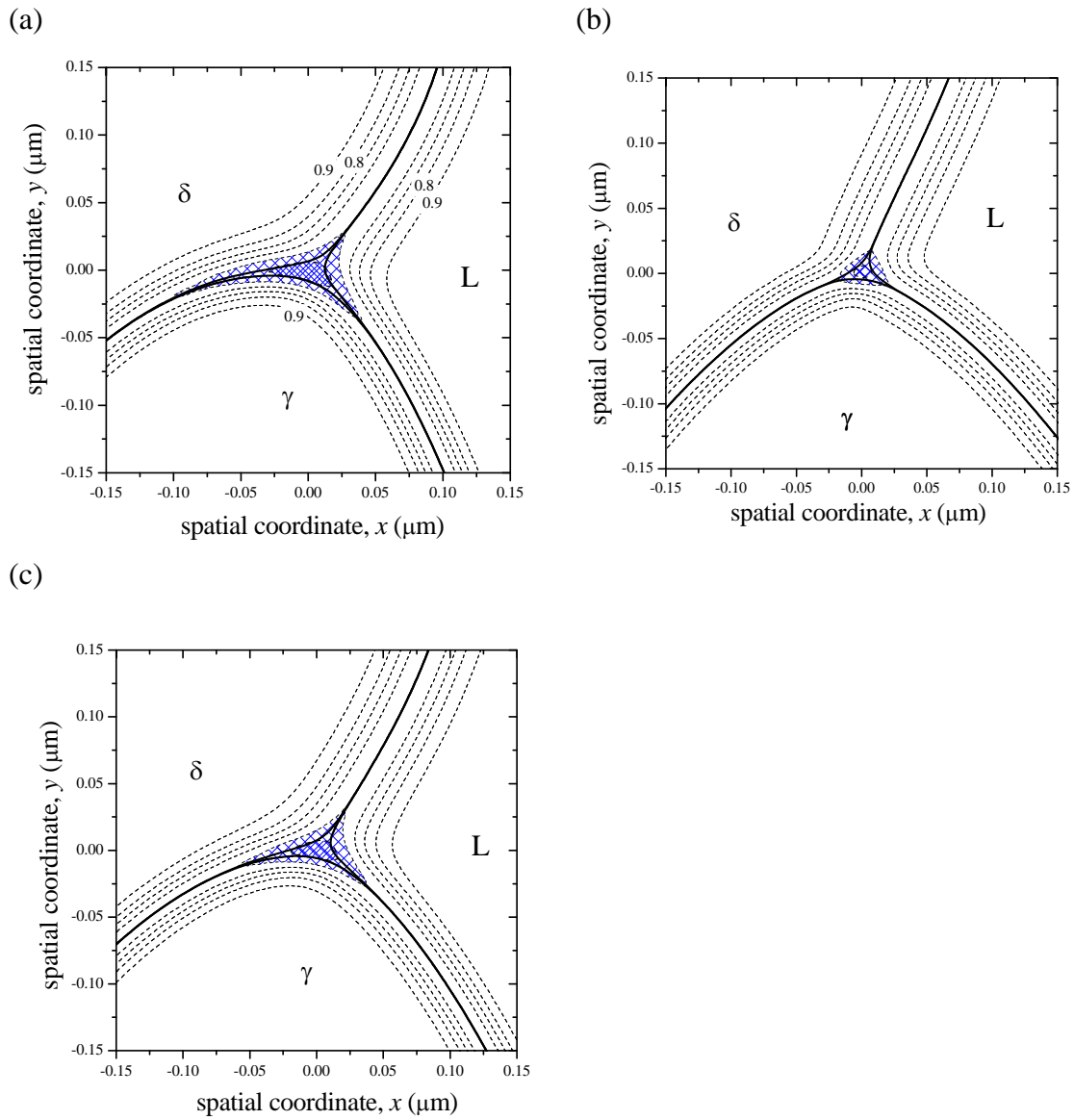
(a)

(b)

(c)

Fig. 4. Contour lines (dashed lines) for the square sum of phase fields, p_s, near the triple junction during the peritectic reaction, calculated (a) without the additional potential, (b) with $n=1.4$ and (c) with $n=2.0$. In each figures, the origin of the spatial coordinates correspond to the position of the triple junction ($p_L=p_\delta=p_\gamma=1/3$). The interval of the contour lines is $\Delta p_s=0.1$. The cross-hatched region indicates the region where $p_s \leq 0.5$. The solid lines represent the level 0.5 contour lines of the phase fields.
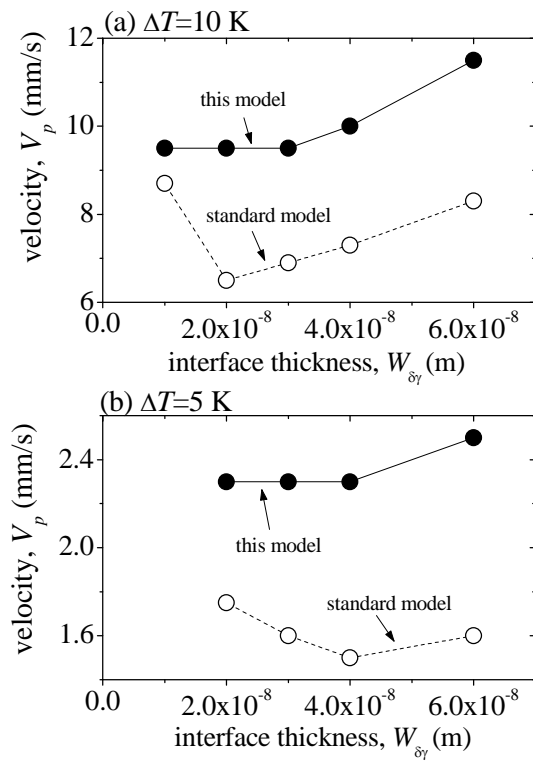
Fig. 5. Convergence behavior of the velocity of growing γ phase with respect to the interface thickness, $W_{\gamma\delta}$, calculated for (a) ΔT=10 K and (b) ΔT=5K. The full and open symbols represent the results obtained by the present model and the standard model, respectively.
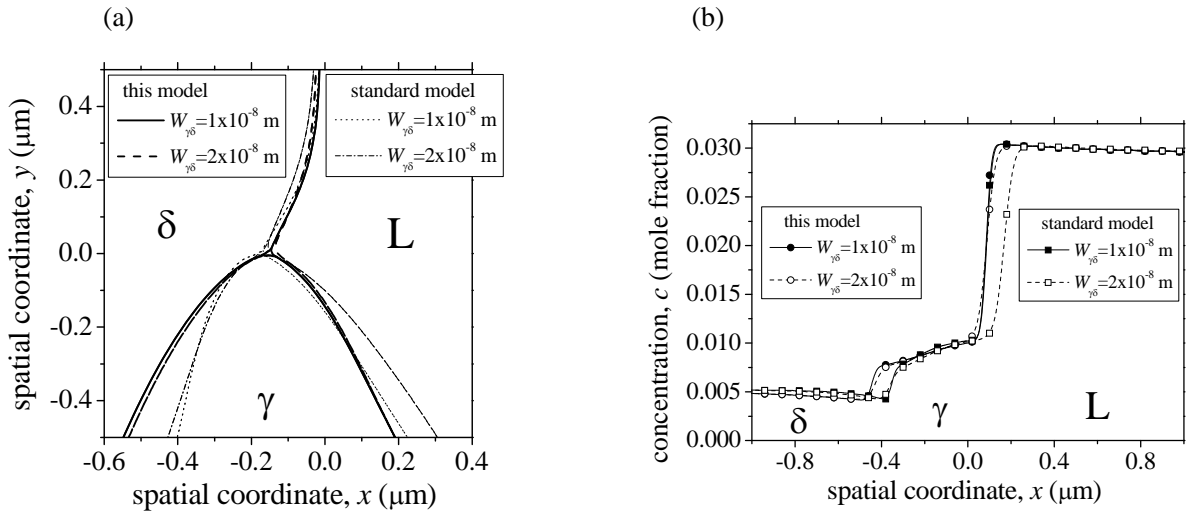
Fig. 6. (a) Level 0.5 contours of phase fields in the steady state at ΔT=10 K. (b) Concentration profiles along x direction at y=−0.3 μm in Fig. (a). For visual aid, one out of every 8 symbols is shown for each profile.

Supplementary Material

A. Dependence of f_{pot} on n and w_{tri}

B. Difference in convergence behavior between the cases of equal and unequal interfacial energies

Munekazu Ohno and Kiyotaka Matsuura

Division of Materials Science and Engineering, Faculty of Engineering, Hokkaido University, Sapporo, Hokkaido, 060-8628, Japan

May 24, 2010

A. Dependence of f_{pot} on n and w_{tri}

The Ginzburg-Landau-type free energy functional in the present model is described in eq.(5). The potential barrier between the bulk phases, f_{pot}, is written as follows,

$$f_{pot} = \left(2\sum_{i,j>i} p_i^2 p_j^2 \right)^{-1} \left(\sum_{i,j>i} \omega_{ij} \cdot p_i^2 p_j^2 + \omega_{tri} \cdot \left(p_i p_j p_k \right)^n \right) \left[\sum_i p_i^2 \left(1 - p_i \right)^2 \right], \quad \text{(S-1)}$$

where ω_{ij} denotes the two-phase potential height between i and j phases. In eq.(S-1), the term, $\omega_{tri} \cdot \left(p_i p_j p_k \right)^n$, represents the additional potential. The contribution of the additional potential to f_{pot} is entirely determined by the values of n and ω_{tri}. Here, we show the dependence of f_{pot} on the values on n and ω_{tri}.

As discussed in the section 2.3, ω_{ij} can be calculated as follows,

$$\omega_{ij} = \frac{3\sqrt{2} \cdot \sigma_{ij}}{W_{ij}}, \quad \text{(S-2)}$$

where σ_{ij} and W_{ij} are the interfacial energy and the interface thickness for i-j interface, respectively. Here, we used the values of σ_{ij} listed in Table 1. The interface thicknesses were set to be $W_{\gamma\delta}=1\times10^{-8}$m and $W_{\delta L}=\sigma_{\gamma\delta}W_{\gamma\delta}/\sigma_{\delta L}$ and $W_{\gamma L}=\sigma_{\gamma\delta}W_{\gamma\delta}/\sigma_{\gamma L}$. Figure S1 shows the contour lines of f_{pot} calculated without the additional potential. The contour lines were drawn in the Gibbs simplex. The Gibbs simplex is the equilateral triangle, where each vertex represents the different phase, δ, γ or liquid. The value of the phase field is determined by the distance to the edge opposite to the corresponding vertex [20]. The interval of the contour lines is $\Delta f_{\text{pot}}=5\times10^5$ J/m^3. The local minima exist at each vertex. The two-phase potential height (the maximum value on the edge) is the highest at the γ-δ edge and is the lowest at the δ-L edge. The global maximum exists not at the γ-δ edge but inside the simplex, a point very close to the γ-δ edge, although it cannot be clearly seen in Fig. S1. It is noted that the maximum value is not significantly higher than the two-phase potential height for the γ-δ interface. As described in the section 4, the p_L profile exhibits the "spike" in the γ-δ interface when the additional potential is not introduced.

For convenience, we introduce the parameter, $\omega^* = \omega_{\delta L} + \omega_{\gamma L} + \omega_{\gamma\delta}$. Figure S2 shows the potential surfaces of f_{pot} calculated for $\omega_{tri}=\omega^*$ and n=1.1, 1.4, 2.0 and 3.0. The potential surface for n=3.0(Fig. S2(d)) is not substantially different from the one without the additional potential shown in Fig. S1. As the value of n decreases, the maximum value increases and the maximum point gradually moves toward the center, namely, $p_L=p_\delta=p_\gamma=1/3$. Figure S3 represents the potential surfaces calculated for n=2.0

and $\omega_{tri}=2\omega^*$, $3\omega^*$ and $7\omega^*$. As the value of ω_{tri} increases, the maximum value increases and the maximum point gradually moves toward the center.

From Figs. S1-S3, one can grasp that the decrease in n and/or the increase in ω_{tri} raises the potential height for the mixture state of three phases. Therefore, the formation of the extra phase can be suppressed by using the small value of n and the large value of ω_{tri} in the present model. As shown in Fig. 2, we can improve the convergence behavior of the peritectic reaction rate with respect to the interface thickness by increasing the contribution of the additional potential. Therefore, we generally expect that the combination of the small value of n and the large value of ω_{tri} yields the excellent result.

As shown in Figs. S2 and S3, the variation of the potential surface f_{pot} due to the increment of ω_{tri} is similar to that due to the decrement of n. Hence, in our preliminary calculations, the value of ω_{tri} was fixed to be $\omega_{tri}=\omega^*$ and different values of n were tested. When we tried $n=1.2$ and 1.3 with $\omega_{tri}=\omega^*$, the calculations were not stable in the present condition. Since the calculation for $n=1.4$ and $\omega_{tri}=\omega^*$ yields the reasonable convergence behavior without the formation of the extra phase, we employed $n=1.4$ and $\omega_{tri}=\omega^*$ in the present study.

It is noted that the formation of the extra phase originates from the difference in σ_{ij} and thus the difference in ω_{ij}. From eq.(S-2), one can comprehend that the difference in ω_{ij} increases with the decrease in W_{ij}. Figure S4 shows the spatial profiles of p_{L} across the $\gamma-\delta$ interface far from the triple junction, calculated without the additional potential ($n=0.0$) for $\Delta T=10$ K. It is seen that as $W_{\gamma\delta}$ decreases, the peak profile becomes sharp and the peak position moves toward the center position of the γ-δ interface. Importantly, the peak value increases with the decrease in $W_{\gamma\delta}$. Hence, the problem with the formation of the extra phase cannot be removed only by the reduction of the interface thickness.
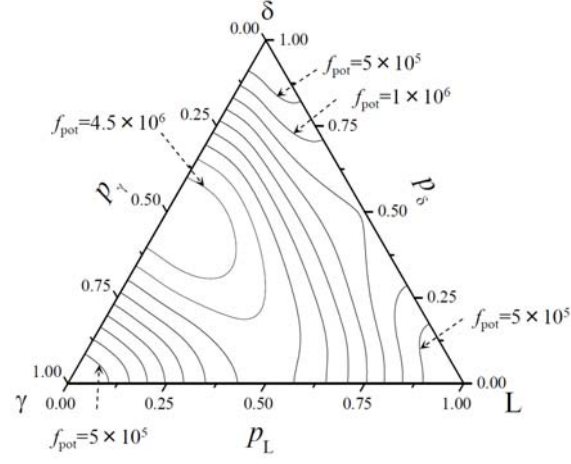
Fig. S1. Potential surface of f_{pot} in the Gibbs simplex. The interval of the contour lines is $\Delta f_{pot}=5\times10^5$ J/m^3. The additional potential is not introduced.

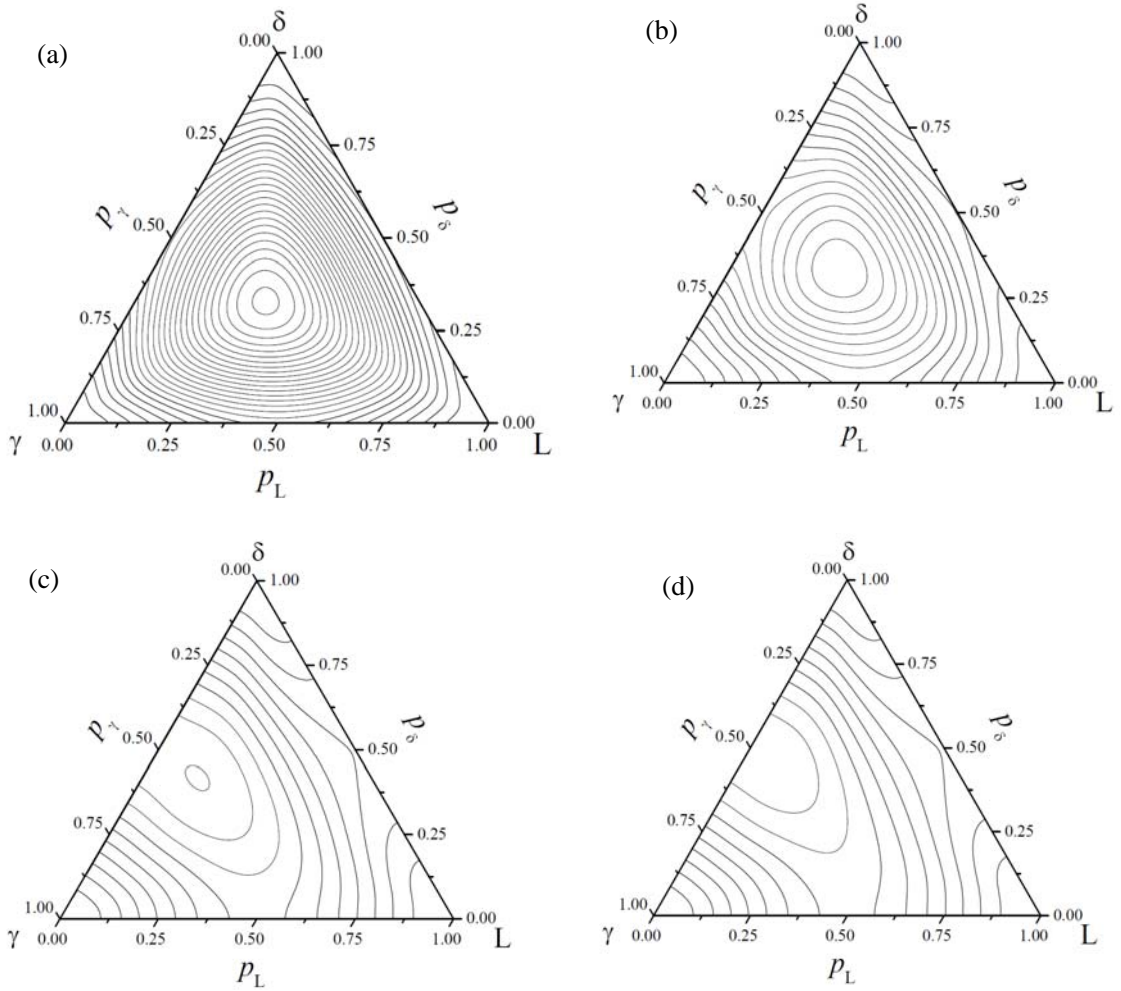Fig. S2. Potential surfaces of f_{pot} in the Gibbs simplex calculated for $\omega_{tri}=\omega^*$ and (a) $n=1.1$, (b) $n=1.4$, (c) $n=2.0$ and (d) $n=3.0$. In each figure, the interval of the contour lines is $\Delta f_{pot}=5\times10^5$ J/m^3.
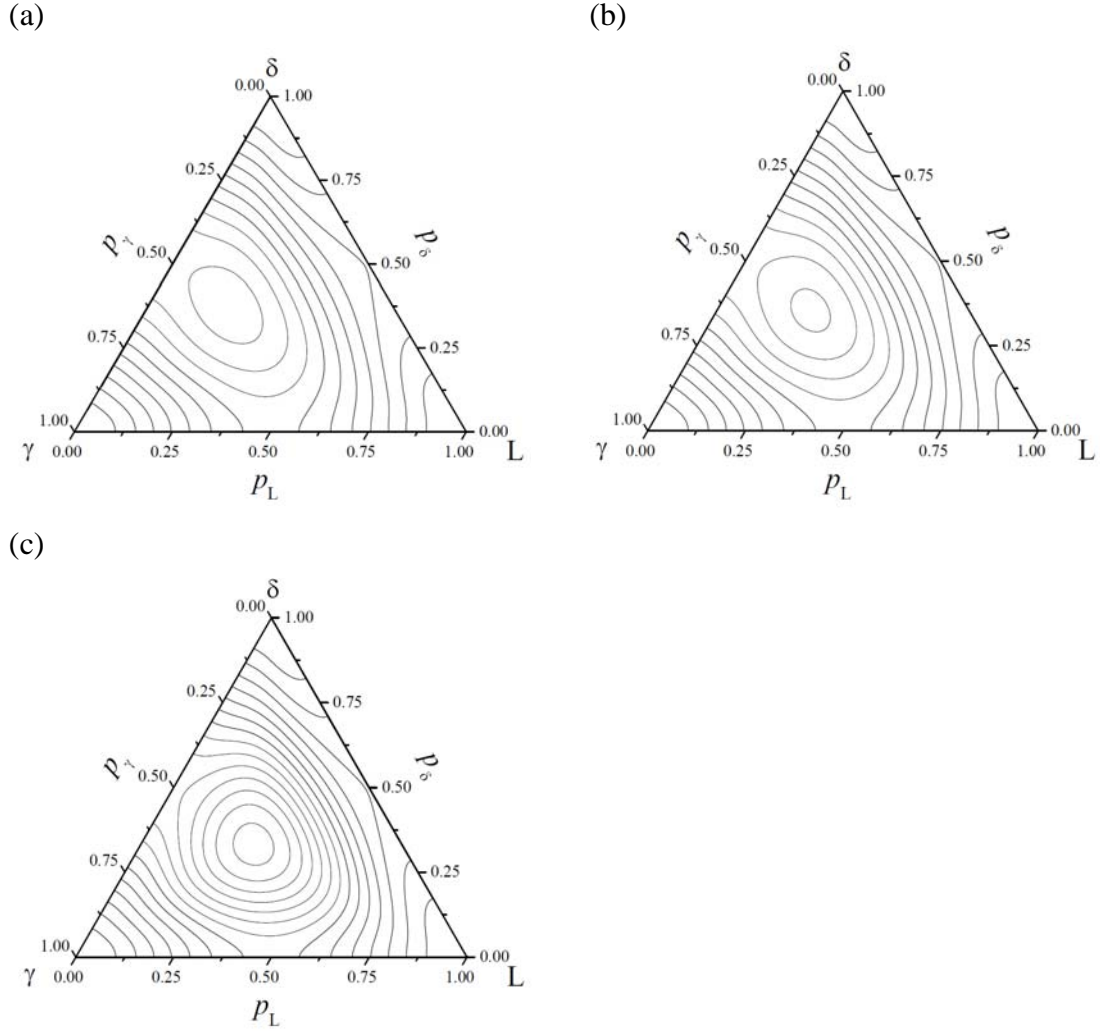
(a)

(b)

(c)

Fig. S3. Potential surfaces of f_{pot} in the Gibbs simplex calculated for $n=2.0$ and (a) $\omega_{tri}=2\omega^*$, (b) $\omega_{tri}=3\omega^*$ and (c) $\omega_{tri}=7\omega^*$. In each figure, the interval of the contour lines is $\Delta f_{pot}=5\times10^5$ J/m^3.
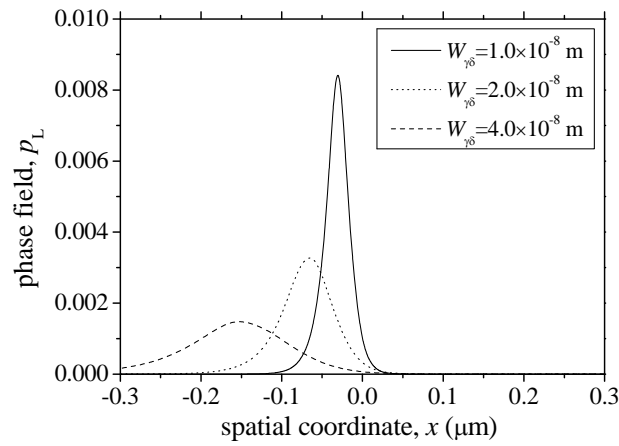

Fig. S4. Spatial profiles of p_L across γ-δ interface along x direction calculated without the additional potential for different values of $W_{\gamma\delta}$. The origin of the horizontal axis corresponds to the center position of γ-δ interface.

B. Difference in convergence behavior between the cases of equal and unequal interfacial energies

In the early works for the quantitative phase-field modeling [11, 13, 20, 21], the effects of thin-interface corrections were discussed based on the convergence curve with respect to W/d_0 where d_0 is the chemical capillary length. In the present model, the chemical capillary length depends on the type of interface as expressed by $d_{0,ij}$. $W_{ij}/d_{0,ij}$ is calculated in this model as follows,

$$\frac{W_{ij}}{d_{0,ij}} = \frac{3\sqrt{2}RT_{m,ij}}{v_m\omega_{ij}}\left(1-k_{ij}\right)\left(c_{j,e}^i - c_{i,e}^j\right). \qquad \text{(S-3)}$$

When the simulations for the unequal interfacial energy and the conditions $\Delta T=10$ K and $W_{\gamma\delta}\leq3.0\times10^{-8}$m are considered (Fig. 4), the values of $W_{ij}/d_{0,ij}$ are always less than 10.2 for the δ-L interface, 2.9 for the γ-L interface and 0.36 for the γ-δ interface. Also, in the calculations for $\Delta T=5$ K and $W_{\gamma\delta}\leq4.0\times10^{-8}$m, the values of W/d_0 are less than 12.3 for the δ-L interface, 3.4 for the γ-L interface and 0.50 for the γ-δ interface. Judging from the convergence curves reported in the early works [11,13,21], these values of $W_{ij}/d_{0,ij}$ corresponds to relatively small values where one can generally expect the well converged result. In fact, almost the constant value is observed in Fig. 4. However, the results for the equal interfacial energies seem to be not converged even for the smallest value of $W_{\gamma\delta}$ used in this study. This point is discussed here.

Figure 2 shows that the convergence of the results for the equal interfacial energy is slower than that for the unequal interfacial energy. The steady state shape of the interfaces near the triple junction at $\Delta T=10$ K is shown in Fig. S5(a). These are the results for the equal interfacial energy. One sees that the steady state shape is not well converged in the range of $W_{\gamma\delta}$ tested here. The steady state shape for the equal interfacial energy is compared with that for the unequal interfacial energy in Fig. S5(b). The curvatures of γ–δ and γ–L interfaces near the junction in the former case are larger than those in the latter case, as is expected from the balance between the interfacial energies near the junction (Young's rule). The velocity of growing γ phase (peritectic reaction rate) for the equal interfacial energy is much higher than the one for unequal interfacial energy as is seen in Fig. 2. Therefore, the peritectic reaction for the equal interfacial energy involves the relatively large curvatures and the high migration velocities of the interfaces. The anomalous interface effect becomes significant in this situation, as is realized from the asymptotic analysis [13, 21]. This should be the reason why the convergence of the results for the equal interfacial energy is slow.
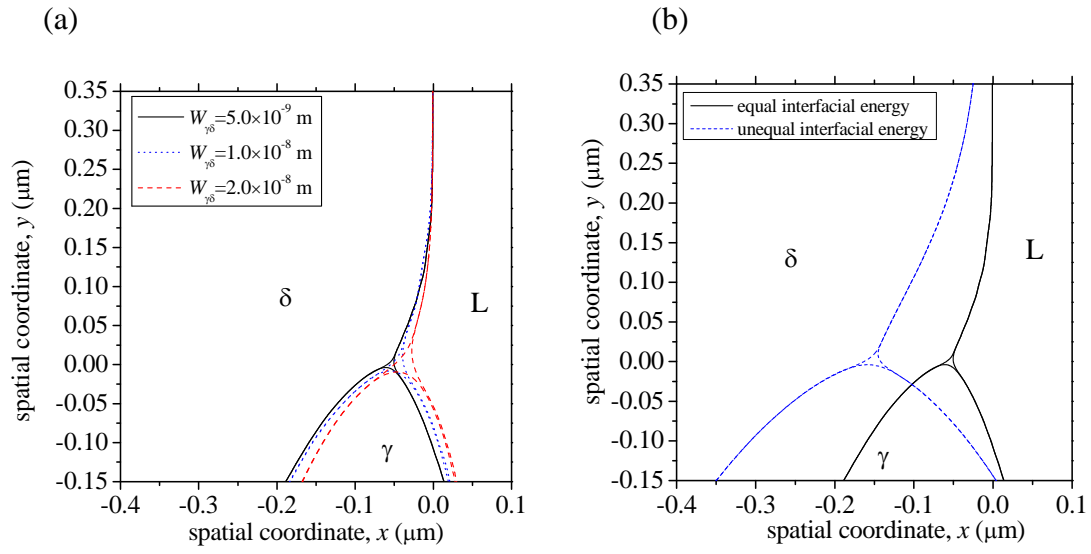
Fig. S5. (a) Steady state shapes of the interfaces near the triple junction at ΔT=10 K for the case of equal interfacial energy. (b) Comparison between the steady state shapes near the triple junction for equal interfacial energy (solid line) and unequal interfacial energy (dashed line). The interface thickness $W_{\gamma\delta}$ is 5.0×10^{-9}m for the former case and 1.0×10^{-8}m for the latter case. In each figure, the origin of y axis is the position of the triple junction and the origin of x axis corresponds to the initial position of L-δ interface.